EXPLAINING EXTREME EVENTS OF 2016

From A Climate Perspective

Special Supplement to the
Bulletin of the American Meteorological Society
Vol. 99, No. 1, January 2018

EXPLAINING EXTREME EVENTS OF 2016 FROM A CLIMATE PERSPECTIVE

Editors

Stephanie C. Herring, Nikolaos Christidis, Andrew Hoell, James P. Kossin,
Carl J. Schreck III, and Peter A. Stott

Special Supplement to the

Bulletin of the American Meteorological Society

Vol. 99, No. 1, January 2018

American Meteorological Society

Corresponding Editor:

Stephanie C. Herring, PhD
NOAA National Centers for Environmental Information
325 Broadway, E/CC23, Rm 1B-131
Boulder, CO 80305-3328
E-mail: stephanie.herring@noaa.gov

Cover credit:

©The Ocean Agency / XL Catlin Seaview Survey / Chrisophe Bailhache—A panoramic image of coral bleaching at Lizard Island on the Great Barrier Reef, captured by The Ocean Agency / XL Catlin Seaview Survey / Christophe Bailhache in March 2016.

HOW TO CITE THIS DOCUMENT

Citing the complete report:

Herring, S. C., N. Christidis, A. Hoell, J. P. Kossin, C. J. Schreck III, and P. A. Stott, Eds., 2018: Explaining Extreme Events of 2016 from a Climate Perspective. *Bull. Amer. Meteor. Soc.*, **99** (1), S1–S157.

Citing a section (example):

Quan, X.W., M. Hoerling, L. Smith, J. Perlwitz, T. Zhang, A. Hoell, K. Wolter, and J. Eischeid, 2018: Extreme California Rains During Winter 2015/16: A Change in El Niño Teleconnection? [in "Explaining Extreme Events of 2016 from a Climate Perspective"]. *Bull. Amer. Meteor. Soc.*, **99** (1), S54–S59, doi:10.1175/BAMS-D-17-0118.1.

EDITORIAL AND PRODUCTION TEAM

Riddle, Deborah B., Lead Graphics Production, NOAA/NESDIS National Centers for Environmental Information, Asheville, NC

Love-Brotak, S. Elizabeth, Graphics Support, NOAA/NESDIS National Centers for Environmental Information, Asheville, NC

Veasey, Sara W., Visual Communications Team Lead, NOAA/NESDIS National Centers for Environmental Information, Asheville, NC

Fulford, Jennifer, Editorial Support, Telesolv Consulting LLC, NOAA/NESDIS National Centers for Environmental Information, Asheville, NC

Griffin, Jessicca, Graphics Support, Cooperative Institute for Climate and Satellites-NC, North Carolina State University, Asheville, NC

Misch, Deborah J., Graphics Support, Telesolv Consulting LLC, NOAA/NESDIS National Centers for Environmental Information, Asheville, NC

Osborne, Susan, Editorial Support, Telesolv Consulting LLC, NOAA/NESDIS National Centers for Environmental Information, Asheville, NC

Sprain, Mara, Editorial Support, LAC Group, NOAA/NESDIS National Centers for Environmental Information, Asheville, NC

Young, Teresa, Graphics Support, Telesolv Consulting LLC, NOAA/NESDIS National Centers for Environmental Information, Asheville, NC

TABLE OF CONTENTS

ABSTRACT—Stephanie C. Herring, Nikolaos Christidi, Andrew Hoell, James P. Kossin, Carl J. Schreck III, and Peter A. Stott

This sixth edition of explaining extreme events of the previous year (2016) from a climate perspective is the first of these reports to find that some extreme events were not possible in a preindustrial climate. The events were the 2016 record global heat, the heat across Asia, as well as a marine heat wave off the coast of Alaska. While these results are novel, they were not unexpected. Climate attribution scientists have been predicting that eventually the influence of human-caused climate change would become sufficiently strong as to push events beyond the bounds of natural variability alone. It was also predicted that we would first observe this phenomenon for heat events where the climate change influence is most pronounced. Additional retrospective analysis will reveal if, in fact, these are the first events of their kind or were simply some of the first to be discovered.

Last year, the editors emphasized the need for additional papers in the area of "impacts attribution" that investigate whether climate change's influence on the extreme event can subsequently be directly tied to a change in risk of the socio-economic or environmental impacts. Several papers in this year's report address this challenge, including Great Barrier Reef bleaching, living marine resources in the Pacific, and ecosystem productivity on the Iberian Peninsula. This is an increase over the number of impact attribution papers than in the past, and are hopefully a sign that research in this area will continue to expand in the future.

Other extreme weather event types in this year's edition include ocean heat waves, forest fires, snow storms, and frost, as well as heavy precipitation, drought, and extreme heat and cold events over land. There were a number of marine heat waves examined in this year's report, and all but one found a role for climate change in increasing the severity of the events. While human-caused climate change caused China's cold winter to be less likely, it did not influence U.S. storm Jonas which hit the mid-Atlantic in winter 2016.

As in past years, the papers submitted to this report are selected prior to knowing the final results of whether human-caused climate change influenced the event. The editors have and will continue to support the publication of papers that find no role for human-caused climate change because of their scientific value in both assessing attribution methodologies and in enhancing our understanding of how climate change is, and is not, impacting extremes. In this report, twenty-one of the twenty-seven papers in this edition identified climate change as a significant driver of an event, while six did not. Of the 131 papers now examined in this report over the last six years, approximately 65% have identified a role for climate change, while about 35% have not found an appreciable effect.

Looking ahead, we hope to continue to see improvements in how we assess the influence of human-induced climate change on extremes and the continued inclusion of stakeholder needs to inform the growth of the field and how the results can be applied in decision making. While it represents a considerable challenge to provide robust results that are clearly communicated for stakeholders to use as part of their decision-making processes, these annual reports are increasingly showing their potential to help meet such growing needs.

7. CMIP5 MODEL-BASED ASSESSMENT OF ANTHROPOGENIC INFLUENCE ON HIGHLY ANOMALOUS ARCTIC WARMTH DURING NOVEMBER–DECEMBER 2016

Jonghun Kam, Thomas R. Knutson, Fanrong Zeng, and Andrew T. Wittenberg

According to CMIP5 simulations, the highly anomalous Arctic warmth during November–December 2016, as estimated in five observed datasets, most likely would not have been possible without anthropogenic forcing.

Introduction. Arctic surface temperatures during November–December 2016 were anomalously warm (Fig. 7.1a). An Arctic area-averaged temperature index (Fig. 7.1b and Fig. ES7.2) set a new high record in the GISS Surface Temperature Analysis data (Hansen et al. 2010), and was either a record high or anomalously high—compared to early 20th century levels—according to four other observational products (online supplement material; Fig. ES7.2; Table ES7.2). Arctic sea ice extent was at record low levels (for the season) during November and December 2016 according to the National Snow and Ice Data Center (NSIDC) website (http://nsidc.org/arcticseaicenews/charctic-interactive-sea-ice-graph/). Arctic sea ice loss has been important for recent Arctic surface temperature amplification (Screen and Simmonds 2010; Kirchmeier-Young et al. 2016).

Here we compare observed Arctic temperature anomalies for 2016 from multiple datasets to CMIP5 model simulations (Taylor et al. 2012) to investigate whether such extreme seasonal warmth would have been likely to occur without anthropogenic forcing. Table ES7.1 lists the 18 CMIP5 models, their run lengths, and ensemble sizes for unforced Control simulations (CMIP5-CONT), Natural Forcing-Only historical simulations (CMIP5-NAT), and All Forcing (natural + anthropogenic) historical simulations (CMIP5-ALL).

AFFILIATIONS: Kam—Department of Civil, Construction, and Environmental Engineering, University of Alabama, Tuscaloosa, Alabama, and Cooperative Institute for Climate Science, Princeton University, Princeton, New Jersey; Knutson, Zeng, and Wittenberg—NOAA/Geophysical Fluid Dynamics Laboratory, Princeton, New Jersey

DOI:10/1175/BAMS-D-17-0115.1

A supplement to this article is available online (10.1175/BAMS-D-17-0115.2)

Data and methods. We assess observed high-latitude warm anomalies for November–December 2016 by defining an observed Arctic temperature index (zonal average over 64°–84°N; Fig. 7.1b; Fig. ES7.2). The index is assumed non-missing for a given year if at least 33% of area has coverage, where coverage at a grid cell requires at least one of the two months to be available. Model data were masked with the GISTEMP observed data availability mask. The GISTEMP dataset uses 1200-km spatial smoothing, resulting in more spatial coverage in the data-sparse Arctic regions, at the expense of relying on the spatial smoothing to fill data gaps. The small region north of 84°N (5.4% of total Arctic area) is not included due to the large fraction of unavailable estimates over the region, especially prior to 1950, even in the smoothed GISTEMP analysis (see Fig. ES7.1). We also analyzed the HadCRUT4 (Morice et al. 2012), NOAA (Vose et al. 2012), Berkeley Earth Land+Ocean (Rohde et al. 2014), and Cowtan & Way version 2.0 (Cowtan and Way 2014) datasets to assess uncertainties in the Arctic temperature index derived from the GISTEMP data (online supplement material).

From the CMIP5 models, we use surface air temperature over land points, and either sea surface temperature or ice surface temperature over ocean points, depending on the simulated sea-ice coverage. The GISTEMP data uses air temperature over land and near-surface water temperature over oceans, with their extrapolation of temperatures being especially prominent over large sea ice regions.

We estimate the fraction of attributable risk (FAR; Stott et al. 2004) for the observed anomalies ($FAR = 1 - P_{nat}/P_{all}$), following the procedures used in our previous regional temperature extremes assessments (e.g., Kam et al. 2016). The FAR analysis begins by assessing the probability of exceeding the second-ranked extreme November–December

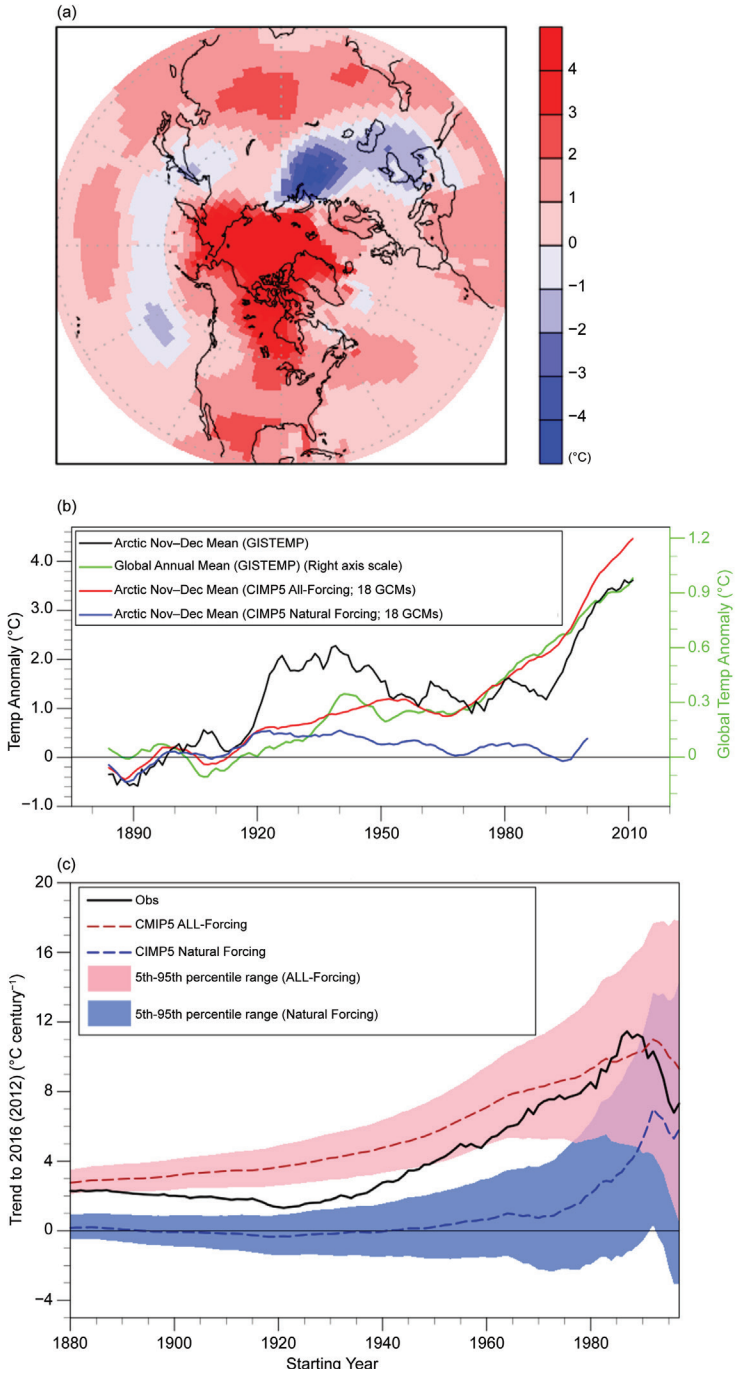

Fig. 7.1. Arctic Nov–Dec 2016 surface temperature anomalies (°C, relative to 1881–1920): (a) GISTEMP observed anomalies; (b) Arctic index (64°–84°N) 10-yr running mean Nov–Dec values. Black curves: observed GISTEMP; red (blue): average of ensemble-means of CMIP5 All-Forcing (Natural-Forcing) anomalies from 18 models, respectively. Green curve: global annual-mean temperature anomalies using the y-axis labels along right edge. (c) Sliding trends (°C century^{-1}) as a function of start years varying from 1880 to 1997. All trends are for data segments ending in 2016 for GISTEMP observations (black curve) or CMIP5 All-Forcing (red curve, with 5th–95th percentile shown by pink shading). Trends end in 2012 for the Natural Forcing-Only data (blue curve and shading). See further details of methods in Fig. ES7.3.

warmth in the Arctic, for both present-day and preindustrial conditions, using 1881–1920 as our reference period. Here, we use the second-ranked year value as our main threshold value since, for GISTEMP, 2016 was the single year that exceeded the second-ranked extreme, and so in determining the probability of a year like 2016, we explore the probability of anomaly exceeding the previous record. We used the first-ranked extreme value as an alternative threshold, as a sensitivity test. The first- and second-ranked extreme values and years for the five observational datasets are presented in Table ES7.2.

For the present-day climate, we estimate the probability of exceeding the second-ranked threshold values, as of the year 2016, in the CMIP5 All-Forcing simulations. A multimodel probability distribution for the All-Forcing (Natural-Forcing) runs is constructed by adding the grand ensemble mean (multimodel mean of the ensemble means from the individual CMIP5 models) to the aggregate distribution of annual anomalies from the CMIP5 control runs. For each individual model, the All-Forcing (Natural-Forcing) distribution consists of the All-Forced (Natural-Forced) ensemble mean for 2016, combined with the distribution of annual anomalies from that model's control run.

For the preindustrial case, we estimate the probability of exceeding the threshold value in the CMIP5 Natural Forcing-Only simulations, extrapolated to 2016. The extrapolated value was based on the ensemble-mean time-mean value from 2001 to the last year of each simulation of the 18 CMIP5 models (2005 or 2012, depending on the model). The probability distributions are computed for each of the eight individual climate models with at least three NAT runs and three All-Forcing runs. All-Forcing runs were extended from 2006 through 2016 using the RCP8.5 scenario. For the multimodel mean, we used the grand ensemble mean from all 18 climate models that provided Natural Forcing-Only runs (including those with a single CMIP5-NAT forcing run).

Lastly, we estimate the observed internal variability by subtracting the grand ensemble mean of the CMIP5–ALL runs from the observations, to attempt to remove the forced variability component. We then filtered the observed residuals using a low-pass filter with a half-power point at nine years, and computed their standard deviation. We also computed the standard deviations of each the eight CMIP5 models' low-passed filtered control run series.

Results. The 10-year moving average of the Arctic November–December temperature index (Fig. 7.1b) shows very strong warming during the early 20th century prior to about 1930. A second major warming period began around 1990, culminating in the 2016 value (Fig. ES7.2) which was the warmest ever recorded in the GISTEMP and Berkeley datasets. In Fig. 7.1b, global-mean annual-mean temperature anomalies are compared with the November–December Arctic temperature index, indicating that in the GISTEMP dataset, Arctic warming over the last century has been almost three times that of observed global mean temperature. Compared to global temperature, the Arctic November–December index also has much more pronounced multidecadal variability. Despite this large multidecadal variability, the observed Arctic warming trend is highly unusual compared to the trends caused by natural variability, according to the average distribution of trends from CMIP5-NAT runs (Fig. 7.1c). This is the case for various trend periods ending in 2012—at least for all trend start years prior to about 1990. The century-scale warming trend and strong multidecadal variability are common features of Arctic temperature indices from a number of observed datasets in addition to GISTEMP (e.g., Fig. ES7.2), including an analysis using only meteorological stations over the region north of 60°N (Bekryaev et al. 2010).

While the century-scale Arctic warming observed since the late 1800s resembles that in the CMIP5 All-Forcing ensemble mean (Fig. 7.1b), the latter does not show the strong warm phase during 1920–40, suggesting that this observed warming may contain a large contribution from internal climate variability [e.g., the Atlantic multidecadal oscillation (Johannessen et al. 2015)] in addition to a contribution of anthropogenic forcing (Najafi et al. 2015; Fyfe et al. 2013). The sliding trend analysis (Fig. 7.1c) indicates that observed trends to 2016 beginning from the first half of the 20th century are typically inconsistent (significantly too low), compared to the CMIP5 All-Forcing ensemble. This inconsistency between the observations and the CMIP5 All-Forcing ensemble could be due to a number of factors including: 1) mis-specified or missing climate forcing agents in the models; 2) errors in the model responses to the climate forcings; 3) underestimation of Arctic internal climate variability in the models; or 4) data issues, including problems with comparing modeled and observed Arctic data as discussed above.

We estimate the FAR for the multimodel ensemble for the first- and second-ranked year threshold values. The FAR ranges from 0.96 to 0.99 across the five observational datasets (Fig. 7.2a). A FAR of 1.0 for a particular set of forcings would indicate that that particular forcing set (e.g., anthropogenic forcing) alone is responsible for the entire risk of exceeding the given threshold. We also explore uncertainties in the FAR estimates, by computing the FAR for the second-ranked year threshold value for each individual CMIP5 model. The spread in these FAR estimates indicates the influence of observational uncertainties as well as uncertainties across the models. The lowest FAR estimate (0.82) is from a combination of the second-ranked year value from NOAA observations and the CSIRO-Mk3-6-0 model (Fig. 7.2a), and reflects that model having the weakest 2016 All-Forcing response among the eight models, along with the second-highest 2016 Natural Forcing-Only response. Most of the individual model FAR estimates in Fig. 7.2a are above 0.9, however.

We evaluate the modeled vs. estimated observed internal decadal variability of Arctic November–December temperatures in Fig. 7.2b. The GFDL-CM3 model's (M4) standard deviation (0.78°C) exceeds the observed estimated range of 0.62°C (Berkeley Earth) to 0.77°C (HadCRUT4). The remaining model control runs have weaker simulated decadal variability than observed, ranging from 0.45° to 0.58°C. Due to the relatively short observational record, and uncertainties in the forced response mean, the estimate of real-world decadal internal variability remains uncertain (e.g., Knutson et al. 2016), and will require further evaluation in the future, for example with paleoclimate data (e.g., Delworth and Mann 2000). The strong intrinsic variability of GFDL-CM3 contributes to its having the second-lowest FAR estimate (for the second-ranked threshold value) among the eight climate models (Fig. 7.2a). Further study is needed to assess the causes of possible under/over-estimates of internal decadal Arctic variability, and to address other caveats and uncertainties identified above.

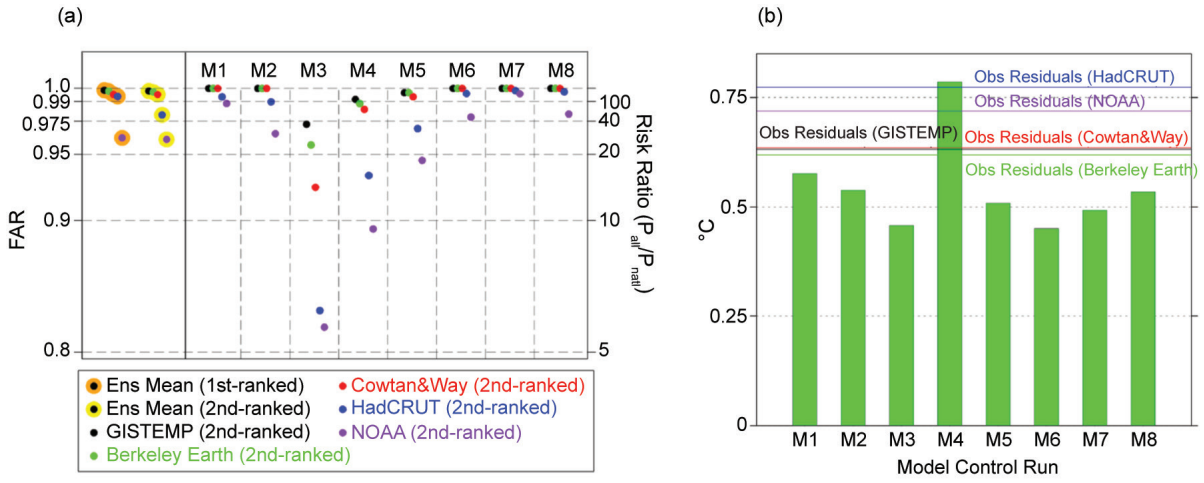

Fig. 7.2. (a) Estimated FAR of exceeding the first- and second-ranked observed Arctic Nov–Dec temperature anomaly thresholds (large orange and yellow circles, respectively), based on the CMIP5 multimodel ensemble. Small dots indicate the observational dataset used. Columns M1–M8 show estimates from individual CMIP5 models (second-ranked observed anomaly threshold) for each observational dataset. (M1–M8 correspond to the model IDs in Table ES7.1.) Risk ratios are indicated by the y-axis labels along right edge. (b) Simulated internal decadal standard deviation of M1–M8 control runs (green bars), along with observational-based estimates from low-pass-filtered Nov–Dec Arctic temperatures (°C) from five observational datasets (horizontal colored lines), with the model-estimated All-Forcing (natural + anthropogenic) response removed.

Conclusions. In summary, we find highly anomalous surface warmth over the Arctic during November-December 2016 in five observed datasets. According to CMIP5 model simulations, this anomalous Arctic warmth most likely would not have been possible without a long-term warming contribution from anthropogenic forcing.

ACKNOWLEDGMENTS. We thank the WCRP's Working Group on Coupled Modeling and the CMIP5 project, for making available the CMIP5 data; and the Hadley Centre and NASS/GISS for providing observational datasets. This study was partly funded by NOAA grant NA14OAR4320106.

REFERENCES

Bekryaev, R. V., I. V. Polyakov, and V. A. Alexeev, 2010: Role of polar amplification in long-term surface air temperature variations and modern Arctic warming. *J. Climate*, **23**, 3888–3906, doi:10.1175/2010JCLI3297.1.

Cowtan, K., and R. G. Way, 2014: Coverage bias in the HadCRUT4 temperature series and its impact on recent temperature trends. *Quart. J. Roy. Meteor. Soc.*, **140**, 1935–1944, doi:10.1002/qj.2297.

Delworth, T. L., and M. E. Mann, 2000: Observed and simulated multidecadal variability in the Northern Hemisphere. *Climate Dyn.*, **16**, 661–676, doi:10.1007/s003820000075.

Fyfe, J. C., K. von Salzen, N. P. Gillett, V. K. Arora, G. M. Flato, and J. R. McConnell, 2013: One hundred years of Arctic surface temperature variation due to anthropogenic influence. *Sci. Rep.*, **3**, 2645, doi:10.1038/srep02645.

Hansen, J., R. Ruedy, M. Sato, and K. Lo, 2010: Global surface temperature change. *Rev. Geophys.*, **48**, RG4004, doi:10.1029/2010RG000345.

Johannessen, O. M., S. I. Kuzmina, L. P. Bobylev, and M. W. Miles, 2016: Surface air temperature variability and trends in the Arctic: New amplification assessment and regionalisation. *Tellus A*, **68**, 28234, doi:10.3402/tellusa.v68.28234.

Kam, J., T. R. Knutson, F. Zeng, and A. T. Wittenberg, 2016: Multimodel assessment of anthropogenic influence on record global and regional warmth during 2015 [in "Explaining Extreme Events of 2015 from a Climate Perspective"]. *Bull. Amer. Meteor. Soc.*, **97** (12), S4–S8, doi:10.1175/bams-d-16-0138.1.

Kirchmeier-Young, M. C., F. W. Zwiers, and N. P. Gillett, 2016: Attribution of extreme events in Arctic sea ice extent. *J. Climate*, **30**, 553–571, doi:10.1175/JCLI-D-16-0412.1.

Knutson, T. R., R. Zhang, and L. W Horowitz, 2016: Prospects for a prolonged slowdown in global warming in the early 21st century. *Nat. Comm.*, **7**, 13676, doi:10.1038/ncomms13676.

Morice, C. P., J. J. Kennedy, N. A. Rayner, and P. D. Jones, 2012: Quantifying uncertainties in global and regional temperature change using an ensemble of observational estimates: The HadCRUT4 data set. *J. Geophys. Res.*, **117**, D08101, doi:10.1029/2011JD017187.

Najafi, M. R., F. W. Zwiers, and N. P. Gillett, 2015: Attribution of Arctic temperature change to greenhouse-gas and aerosol influences. *Nat. Clim. Change*, **5**, 246–249, doi:10.1038/nclimate2524.

Rohde, R., and Coauthors, 2014: A new estimate of the average Earth surface land temperature spanning 1753 to 2011. *Geoinfo. Geostat. Overv.*, **1** (1), doi:10.4172/2327-4581.1000101.

Screen, J. A., and I. Simmonds, 2010: The central role of diminishing sea ice in recent Arctic temperature amplification. *Nature*, **464**, 1334–1337, doi:10.1038/nature09051.

Stott, P. A., D. A. Stone, and M. R. Allen, 2004: Human contribution to the European heatwave of 2003. *Nature*, **432**, 610–614, doi:10.1038/nature03089.

Taylor, K. E., R. J. Stouffer, and G. A. Meehl, 2012: An overview of CMIP5 and the experimental design. *Bull. Amer. Meteor. Soc.,* **93**, 485–498, doi:10.1175/BAMS-D-00094.1.

Vose, R. S., and Coauthors, 2012: NOAA's merged land–ocean surface temperature analysis. *Bull. Amer. Meteor. Soc.*, **93**, 1677–1685, doi:10.1175/BAMS-D-11-00241.1.

Table 1.1. SUMMARY of RESULTS

ANTHROPOGENIC INFLUENCE ON EVENT			
	INCREASE	**DECREASE**	**NOT FOUND OR UNCERTAIN**
Heat	Ch. 3: Global Ch. 7: Arctic Ch. 15: France Ch. 19: Asia		
Cold		Ch. 23: China Ch. 24: China	
Heat & Dryness	Ch. 25: Thailand		
Marine Heat	Ch. 4: Central Equatorial Pacific Ch. 5: Central Equatorial Pacific Ch. 6: Pacific Northwest Ch. 8: North Pacific Ocean/Alaska Ch. 9: North Pacific Ocean/Alaska Ch. 9: Australia		Ch. 4: Eastern Equatorial Pacific
Heavy Precipitation	Ch. 20: South China Ch. 21: China (Wuhan) Ch. 22: China (Yangtze River)		Ch. 10: California (failed rains) Ch. 26: Australia Ch. 27: Australia
Frost	Ch. 29: Australia		
Winter Storm			Ch. 11: Mid-Atlantic U.S. Storm "Jonas"
Drought	Ch. 17: Southern Africa Ch. 18: Southern Africa		Ch. 13: Brazil
Atmospheric Circulation			Ch. 15: Europe
Stagnant Air			Ch. 14: Western Europe
Wildfires	Ch. 12: Canada & Australia (Vapor Pressure Deficits)		
Coral Bleaching	Ch. 5: Central Equatorial Pacific Ch. 28: Great Barrier Reef		
Ecosystem Function		Ch. 5: Central Equatorial Pacific (Chl-***a*** and primary production, sea bird abundance, reef fish abundance) Ch. 18: Southern Africa (Crop Yields)	
El Niño	Ch. 18: Southern Africa		Ch. 4: Equatorial Pacific (Amplitude)
TOTAL	18	3	9

	METHOD USED	Total Events
Heat	Ch. 3: CMIP5 multimodel coupled model assessment with piCont, historicalNat, and historical forcings Ch. 7: CMIP5 multimodel coupled model assessment with piCont, historicalNat, and historical forcings Ch. 15: Flow analogues conditional on circulation types Ch. 19: MIROC-AGCM atmosphere only model conditioned on SST patterns	
Cold	Ch. 23: HadGEM3-A (GA6) atmosphere only model conditioned on SST and SIC for 2016 and data fitted to GEV distribution Ch. 24: CMIP5 multimodel coupled model assessment	
Heat & Dryness	Ch. 25: HadGEM3-A N216 Atmosphere only model conditioned on SST patterns	
Marine Heat	Ch. 4: SST observations; SGS and GEV distributions; modeling with LIM and CGCMs (NCAR CESM-LE and GFDL FLOR-FA) Ch. 5: Observational extrapolation (OISST, HadISST, ERSST v4) Ch. 6: Observational extrapolation; CMIP5 multimodel coupled model assessment Ch. 8: Observational extrapolation; CMIP5 multimodel coupled model assessment Ch. 9: Observational extrapolation; CMIP5 multimodel coupled model assessment	
Heavy Precipitation	Ch. 10: CAM5 AMIP atmosphere only model conditioned on SST patterns and CESM1 CMIP single coupled model assessment Ch. 20: Observational extrapolation; CMIP5 and CESM multimodel coupled model assessment; auto-regressive models Ch. 21: Observational extrapolation; HadGEM3-A atmosphere only model conditioned on SST patterns; CMIP5 multimodel coupled model assessment with ROF Ch. 22: Observational extrapolation, CMIP5 multimodel coupled model assessment Ch. 26: BoM seasonal forecast attribution system and seasonal forecasts Ch. 27: CMIP5 multimodel coupled model assessment	
Frost	Ch. 29: *weather@home* multimodel atmosphere only models conditioned on SST patterns; BoM seasonal forecast attribution system	
Winter Storm	Ch. 11: ECHAM5 atmosphere only model conditioned on SST patterns	
Drought	Ch. 13: Observational extrapolation; weather@home multimodel atmosphere only models conditioned on SST patterns; HadGEM3-A and CMIP5 multimodel coupled model assessent; hydrological modeling Ch. 17: Observational extrapolation; CMIP5 multimodel coupled model assessment; VIC land surface hdyrological model, optimal fingerprint method Ch. 18: Observational extrapolation; *weather@home* multimodel atmosphere only models conditioned on SSTs, CMIP5 multimodel coupled model assessment	
Atmospheric Circulation	Ch. 15: Flow analogues distances analysis conditioned on circulation types	
Stagnant Air	Ch. 14: Observational extrapolation; Multimodel atmosphere only models conditioned on SST patterns including: HadGEM3-A model; EURO-CORDEX ensemble; EC-EARTH+RACMO ensemble	
Wildfires	Ch. 12: HadAM3 atmospere only model conditioned on SSTs and SIC for 2015/16	
Coral Bleaching	Ch. 5: Observations from NOAA Pacific Reef Assessment and Monitoring Program surveys Ch. 28: CMIP5 multimodel coupled model assessment; Observations of climatic and environmental conditions (NASA GES DISC, HadCRUT4, NOAA OISSTV2)	
Ecosystem Function	Ch. 5: Observations of reef fish from NOAA Pacific Reef Assessment and Monitoring Program surveys; visual observations of seabirds from USFWS surveys. Ch. 18: Empirical yield/rainfall model	
El Niño	Ch. 4: SST observations; SGS and GEV distributions; modeling with LIM and CGCMs (NCAR CESM-LE and GFDL FLOR-FA) Ch. 18: Observational extrapolation; *weather@home* multimodel atmosphere only models conditioned on SSTs, CMIP5 multimodel coupled model assessment	
		30